HYDROLOGICAL PROCESSES
Hydrol. Process. **17**, 2929–2945 (2003)
Published online in Wiley InterScience (www.interscience.wiley.com). DOI: 10.1002/hyp.1442

Hydrological regime analysis of the Selenge River basin, Mongolia

X. Ma,[1]* T. Yasunari,[1,2,3] T. Ohata,[2,4] L. Natsagdorj,[5] G. Davaa[5] and D. Oyunbaatar[5]

[1] *Frontier Research System for Global Change, 3173-25 Showa-machi, Kanazawa-ku, Yokohama 236-0001, Japan*
[2] *Frontier Observational Research System for Global Change, 3173-25 Showa-machi, Kanazawa-ku, Yokohama 236-0001, Japan*
[3] *Hydrospheric Atmospheric Research Center, Nagoya University, Nagoya 464-8601, Japan*
[4] *Institute of Low Temperature Science, Hokkaido University, Kita-19, Nishi-8, Kita-ku, Sapporo 060-0819, Japan*
[5] *Institute of Meteorology and Hydrology, Khudaldaany Gudamj 5, Ulaanbaatar 46, Mongolia*

Abstract:

Arid and semi-arid regions are very vulnerable to environmental changes. Climate change studies indicate that the environment in such areas will steadily deteriorate with global warming; inland lakes will shrink and desert areas will expand. Mongolia is a landlocked country in north-central Asia that contains a unique ecological system consisting of taiga, steppe, and desert from north to south. The Selenge River basin (280 000 km^2) in northern Mongolia is a semi-arid region underlain by permafrost, between latitudes 46 and 52°N, and longitudes 96 and 109°E. The issue of sustainable development of the basin is very important owing to its limited natural resources, including fresh water, forest, and rangeland. To examine the water cycle processes in the basin, a hydrological analysis was carried out using a simple scheme for the interaction between the land surface and atmosphere (big-leaf model) coupled to a hydrological model for the period 1988–92 to estimate the hydrological regime of the basin. Annual precipitation in this period averaged 298 mm, ranging from 212 to 352 mm at a $1° \times 1°$ resolution based on data from 10 gauges, and the estimated annual evapotranspiration averaged 241 mm, ranging between 153 and 300 mm. This indicates that evapotranspiration accounts for the overwhelming majority of the annual precipitation, averaging 81% and ranging between 64 and 96%. The annual potential evapotranspiration in the basin averaged 2009 mm; the ratio of evapotranspiration (actual to potential evapotranspiration) was 0·12 and the wetness index (annual precipitation to potential evapotranspiration) was 0·15. Copyright © 2003 John Wiley & Sons, Ltd.

KEY WORDS semi-arid area; hydrological model; water budget component; Selenge River basin

INTRODUCTION

Arid and semi-arid regions cover one-third of the land on Earth (Verstraete and Schwartz, 1991; Renard *et al.*, 1993). Since these regions are sensitive to environmental changes, studies of the interactions between the land surface and atmosphere are of increasing importance (e.g. Manabe *et al.*, 1991; Milly, 1992, 1997; Wetherald and Manabe, 1999, 2003). Arid and semi-arid zones have recently become an important topic of research on climate change (e.g., McMahon, 1988; Michaud and Sorooshian, 1994a,b; Ye *et al.*, 1997; Lange *et al.*, 1999; Andersen *et al.*, 2001; Jothityangkoon *et al.*, 2001). IHP-IV (International Hydrological Programme phase IV from 1990 to 1995) included this issue to give special attention to the hydrological regime changes associated with global climate changes in arid and semi-arid regions.

Mongolia, a landlocked country in north-central Asia, lies on a high plateau surrounded by mountain ridges, in the transition zone between the Siberian taiga and the dry steppes and semi-deserts of central Asia. The country has a distinctly continental climate, with very cold winters and hot summers. According to records, the extreme minimum temperature is $-52{\cdot}9\,°C$ in January and the extreme maximum temperature is $43{\cdot}1\,°C$

* Correspondence to: X. Ma, Frontier Research System for Global Change, 3173-25 Showa-machi, Kanazawa-ku, Yokohama 236-0001, Japan. E-mail: xyma@jamstec.go.jp

Received 19 June 2002
Accepted 7 April 2003

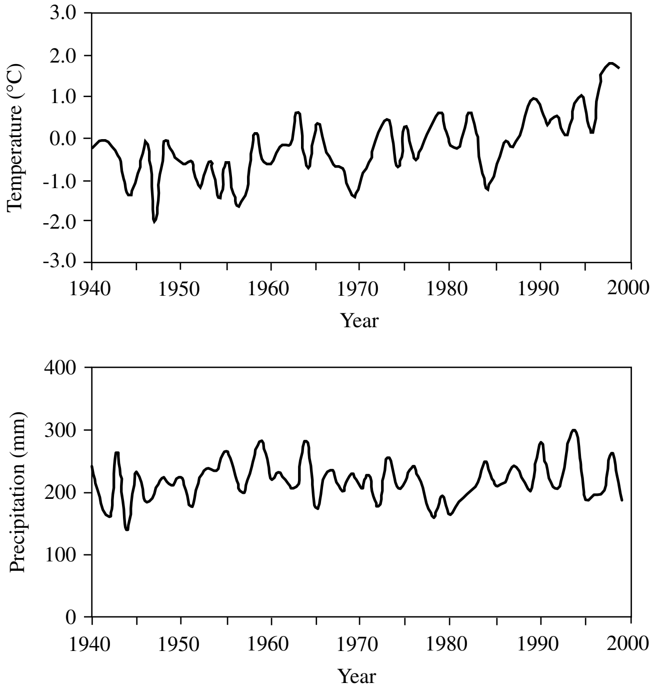

Figure 1. Variation in annual temperature and precipitation in Mongolia over the last 60 years (from Dagvadorj (2000))

(Dagvadorj, 2000). The average temperature in Mongolia has increased approximately 1·56 °C over the last 60 years (Figure 1). This temperature increase has been more prominent in the winter months and in the mountain areas of western and northern Mongolia than it has in the Gobi and steppe areas. An impact assessment was implemented using the IPCC-recommended climate change scenarios for 2039 and 2069 to predict the effects of climate change in Mongolia. This suggested that the desert and steppe zones will expand northwards; the Gobi desert will significantly increase in size by 2039 and 2069, and the area of desert steppe will also increase by 2069 (Dagvadorj and Batjargal, 1999). It is also very possible that the currently permanent snow and glaciers will melt, and that after a period of warming many of the small rivers that are fed by snow, permafrost, and glaciers will disappear. Permafrost occurs in about 63% of Mongolia; according to these climate change scenarios, the area of permafrost will drop to 24–28% by 2040 and 16–25% by 2070.

The Selenge River basin (280 000 km^2) is a semi-arid region located in northern Mongolia between latitudes 46 and 52°N, and longitudes 96 and 109 °E. Most of the basin is covered by forest or grassland and is underlain by permafrost. This densely populated area is the major source of fresh water in Mongolia. The demand for water is increasing annually because of population growth, industrialization, and lifestyle changes. Consequently, much attention is being paid to the hydrological regime changes associated with development and the probable environmental changes in the basin in the near future. No quantitative hydrological analysis of the basin has ever been conducted.

This study examined the hydrological processes of the Selenge River basin using a model comprised of a soil–vegetation–atmosphere transfer (SVAT) scheme combined with a hydrological model (Ma *et al.*, 2000). The next section describes the basin and provides information regarding its location and the datasets used in this study. The third section explains the model, and the fourth section describes the results of the model. The hydrological regime of the basin is analysed in the fifth section. Finally, conclusions are drawn in the sixth section.

BASIN AND HYDROMETEOROLOGICAL DATA

Basin description

The Selenge River basin is located in northern Mongolia, between latitudes 46 and 52°N and longitudes 96 and 109°E, and has an area of 280 000 km^2. It is the source region for the Lake Baikal basin (area 600 000 km^2). It contains two main rivers: the Selenge and Orhon (Figure 2). The basin covers seven provinces (Zavkhan, Khubsgul, Bulgan, Arkhangai, Uvurkhangai, Selenge, and Tuv), and contains the capital city, Ulaanbaatar. The population of the basin is about 1 450 000, which is approximately 70% of the total population of Mongolia (Adyabadam, 1999). The average annual temperature is below freezing. The annual precipitation is about 300 mm (Oyunbaatar, 1999), but the temporal and spatial distribution over the basin is very uneven; during the period 1980–92, it ranged from 147 mm at Murun (no. 231 in Figure 2) in 1980 to 598 mm at Erdenet-Ovoo (no. 236 in Figure 2) in 1985. Although there are no detailed reports of the vegetation distribution for the basin, the World Resources Institute (http://www.wri.org) has reported the land cover for the Lake Baikal basin as 33% forest and 52% grassland.

The basin is shown on a digital map based on the NOAA–GLOBE (global land one-kilometre base elevation) dataset (http://www.ngdc.noaa.gov/seg/topo/globe.shtml). Figure 3 shows the distribution of elevation in the Selenge River basin. The lowest elevation, near the outlet, exceeds 600 m, and the highest, in the Hangyan Mountains, exceeds 3000 m. The elevation is between 1000 and 2000 m in about 72% of the basin. To simulate the water flow in channels, a 0·1° grid map of the river network was derived and, to run the model, meteorological data were interpolated for the whole basin on a 1° × 1° grid.

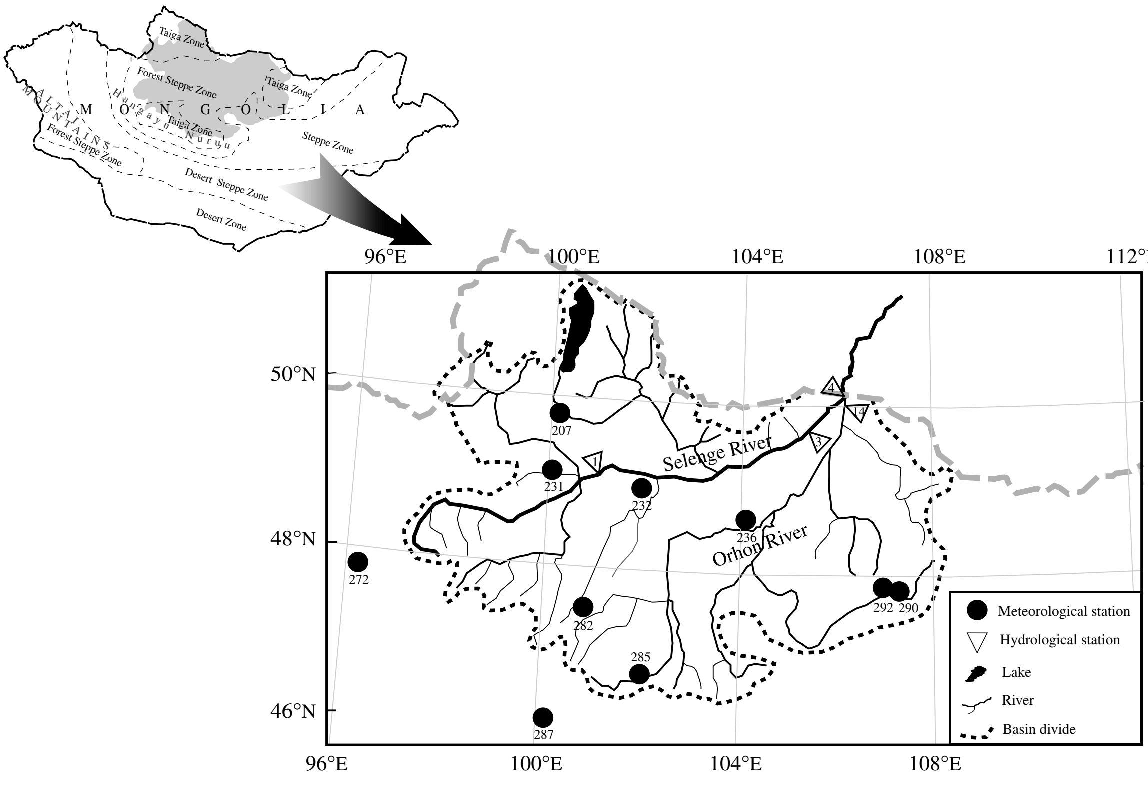

Figure 2. Natural zones in Mongolia and map of the Selenge River basin

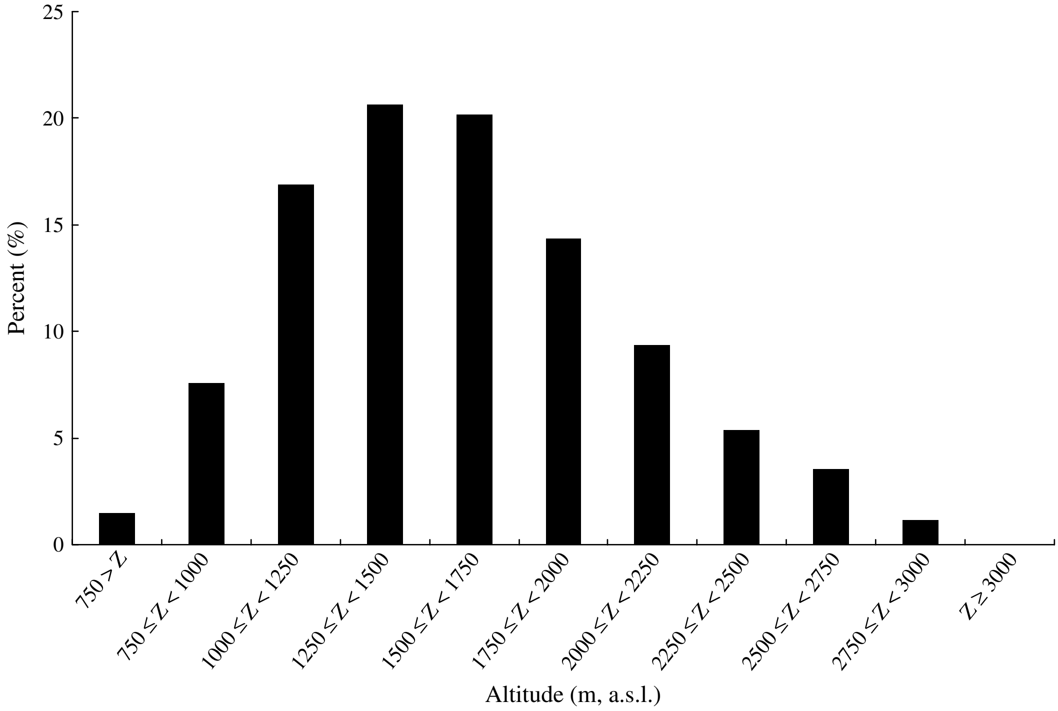

Figure 3. Elevation distribution of the Selenge River basin

Hydrometeorological data

Data for 1988 to 1992 are available from four hydrological stations. Two are located midstream and downstream on the Selenge River, one is located downstream, on the Orhon River, and the fourth is at the outlet. The locations of the gauges are shown in Figure 2. The discharge data were based on measured water levels according to the calibrated relationship between the water level and discharge at a section. The basin outlet is at Sukhbaatar (no. 4 in Figure 2). The study also used data from 10 meteorological gauges: two outside and eight inside the basin. Table I lists information for all of the gauges, and Table II shows the meteorological variables used in the study. Meteorological data were interpolated onto a $1^\circ \times 1^\circ$ grid with the data for the nearest three stations weighted using the inverse of the distance between each grid point and the three gauge locations (Ma *et al.*, 2000).

MODEL DESCRIPTION

A large-scale hydrological model that incorporates land surface processes, including snowmelt, evapotranspiration, and runoff formation, was developed to understand hydrological regimes at the basin scale. The model contained three submodels, i.e. SVAT, runoff, and river-flow-routing models, to examine interactions between the atmosphere and land surface and the water flow over the land.

The study used the SVAT model of Ma *et al.* (1998). The vegetation was described using a single-layer big-leaf model and the soil layer was modelled as being 6 m thick, which is considered the isothermal depth. Radiation components were estimated from the daily routine meteorological data set using the method of Kondo (1994) as follows.

Table I. List of meteorological and hydrological stations used in the study

Number	Name/River	District/Station	Latitude	Longitude	Elevation (m)	Catchment area (km^2)
Meteorological station						
207	Khatgal	Khubsgul	54° 26′	100° 9′	1668	
231	Murun	Khubsgul	49° 38′	100° 10′	1283	
232	Khutag	Bulgan	49° 23′	102° 42′	933	
236	Erdenet-Ovoo	Bulgan	49° 3′	104° 6′	1300	
272	Uliastai	Zavkhan	47° 45′	96° 51′	1751	
282	Tsetserleg	Arkhangai	47° 27′	101° 28′	1693	
285	Khujirt	Uvurkhangai	46° 54′	102° 46′	1650	
287	Bayankhongor	Bayankhongor	46° 8′	100° 41′	1859	
290	Zuunmod	Tuv	47° 43′	106° 57′	1529	
292	Ulaanbaat	Ulaanbaatar	47° 55′	106° 52′	1306	
Hydrological station						
1	Selenge	Ikh-Uul	49° 14′	101° 21′		69 800
3	Selenge	Zuunburen	50° 4′	105° 28′		148 000
4	Selenge	Sukhbaatar	50° 9′	106° 3′		281 700
14	Orhon	Sukhbaatar	50° 10′	106° 5′		132 000

Table II. Daily routine meteorological data used in the study

Item	Unit
Maximum air temperature	°C
Minimum air temperature	°C
Vapour pressure	hPa
Relative humidity	%
Average air pressure	hPa
Average wind speed	m s^{-1}
Precipitation amount	mm
Sunshine duration	h

Global solar radiation

Daily extraterrestrial radiation $S_{\text{od}}^{\downarrow}$ was calculated using:

$$S_{\text{od}}^{\downarrow} = \frac{I_{\text{oo}}}{\pi}\left(\frac{d_{\text{so}}}{d_{\text{s}}}\right)^2 (H_{\text{a}} \sin\phi \sin\delta + \cos\phi \cos\delta \sin H_{\text{a}}) \tag{1}$$

where I_{oo} is the solar constant (1365 W m^{-2}), d_{s} and d_{so} are the distance and average distance from the Earth to the sun respectively, H_{a} is the hour angle, ϕ is the latitude, and δ is the declination. The possible duration of sunshine N_{o} is written as

$$N_{\text{o}} = \frac{2H_{\text{a}}}{0{\cdot}2618} \tag{2}$$

From Equation (2), the amount of global solar radiation $S_{\text{d}}^{\downarrow}$ can be estimated using

$$S_{\text{d}}^{\downarrow} = \begin{cases} S_{\text{od}}^{\downarrow}\left(a + b\frac{N+\Delta N}{N_{\text{o}}}\right), & 0 < \dfrac{N}{N_{\text{o}}} \le 1 \\ c, & \dfrac{N}{N_{\text{o}}} = 0 \end{cases} \tag{3}$$

where N and ΔN are the observed sunshine duration and the corrected value of the sunshine duration (zero) respectively, and a (0·55), b (0·179) and c (0·114) are constants that depend on the sunshine recorder type. Using latitude and the day of the year, d_{so}/d_s, H_a and δ can be calculated as:

$$H_a = \cos^{-1}(-\tan\phi\tan\delta) \tag{4}$$

$$\frac{d_{so}}{d_s} = 1{\cdot}000\,11 + 0{\cdot}034\,221\cos\eta + 0{\cdot}001\,28\sin\eta + 0{\cdot}000\,719\cos 2\eta + 0{\cdot}000\,077\sin 2\eta \tag{5}$$

$$\delta = sin^{-1}(0{\cdot}398\sin\alpha_2) \tag{6}$$

$$\alpha_2 = 4{\cdot}871 + \eta + 0{\cdot}033\sin\eta \tag{7}$$

$$\eta = \frac{2\pi}{365}\mathrm{IDA} \tag{8}$$

$$\mathrm{IDA} = 30{\cdot}36(M_{\mathrm{onth}} - 1) + \mathrm{DAY} \tag{9}$$

where M_{onth} is the month and DAY is the day of the month.

Upward and downward longwave radiation

The upward $L_u^{\uparrow}$ and downward $L_d^{\downarrow}$ longwave radiation can be described, using

$$L_u^{\uparrow} = \varepsilon\sigma T_s^4 \tag{10}$$

$$L_d^{\downarrow} = \sigma T_a^4[1 - (1 - L_{df}^{\downarrow}/\sigma T_a^4)C] \tag{11}$$

where ε is the emissivity (0·97), σ is the Stefan–Boltzmann constant ($5{\cdot}67 \times 10^{-8}$ W m^{-2} K^{-4}), T_s is the land surface temperature, T_a is the air temperature measured 2 m above the land surface, $L_{df}^{\downarrow}$ is the downward longwave radiation on a clear day, and C is a coefficient related to sunshine ratio. $L_{df}^{\downarrow}$ and C can be described using the empirical formula

$$L_{df}^{\downarrow} = (0{\cdot}74 + 0{\cdot}91x + 0{\cdot}07x^2)\sigma T_a^4 \tag{12}$$

$$x = 0{\cdot}0315T_{\mathrm{DEW}} - 0{\cdot}1836 \tag{13}$$

$$T_{\mathrm{DEW}} = \frac{237{\cdot}3\ \log_{10}\left(\dfrac{\mathrm{WVP}}{6{\cdot}11}\right)}{7{\cdot}5 - \log_{10}\left(\dfrac{\mathrm{WVP}}{6{\cdot}11}\right)} \tag{14}$$

Set $A = N/N_o$, if $1 \geqslant A > 0$ then

$$C = 0{\cdot}826A^3 - 1{\cdot}23A^2 + 1{\cdot}135A + 0{\cdot}298 \tag{15}$$

If $A = 0$ then

$$C = 0{\cdot}2235 \tag{16}$$

where WVP is the water vapour pressure and T_{DEW} is the dew point temperature. The net radiation R_n, can be calculated as

$$R_n = (1 - \mathrm{ref})S_d^{\downarrow} - L_u^{\uparrow} + L_d^{\downarrow} \tag{17}$$

where ref is the albedo (0·1 for soil) of the land surface.

Latent and sensible heat fluxes

To estimate the heat fluxes between the land surface and atmosphere, the Penman–Monteith method (Monteith, 1965) was adopted:

$$\ell E = \frac{\Delta(R_n - G) + \rho_a c_a \delta q / r_a}{\Delta + \gamma(1 + r_s/r_a)} \tag{18}$$

$$H = \frac{(R_n - G)\gamma(1 + r_s/r_a) - \rho_a c_a \delta q / r_a}{\Delta + \gamma(1 + r_s/r_a)} \tag{19}$$

where G is the heat flux into the soil or snow layer, Δ is the slope of the saturated vapour pressure curve at air temperature T_a, γ is the psychrometric constant, c_a is the specific heat of the air, ρ_a is the density of air, δq is the specific humidity deficit, r_a is the aerodynamic resistance, and r_s is the surface resistance. The value of G is determined using the soil temperature profile. r_a can be calculated with the assumption of a neutral atmosphere.

To determine r_s, Blyth and Harding (1995) reported the following simple modification of the method of Jarvis (1976):

$$r_s = r_{smin} \exp(\beta \delta q) \tag{20}$$

where r_{smin} is the minimum surface resistance and β is a constant (dimensionless number: 0·046). Ma *et al.* (1999) conducted a detailed study to fit the value of r_{smin}, and found a linear relationship between r_{smin} and the radiation dryness index (RDI), the ratio of the annual net radiation to precipitation for a region, and compared the results derived from different climatic regions with different vegetation communities. Accordingly, r_{smin} is given by

$$r_{smin} = \eta \ \mathrm{RDI} \tag{21}$$

where η is a coefficient (dimensionless number) related to local vegetation conditions and is between 100 and 490.

In this model, the thermal conductive processes for the soil and snow layers were considered separately for different material zones. The conduction equation in the snow layer can be written as

$$c_p \rho_p \frac{\partial T_p}{\partial t} = \frac{\partial}{\partial z}\left(\lambda_p \frac{\partial T_p}{\partial z}\right) - \frac{\partial I_n}{\partial z} - \ell_f F \tag{22}$$

where c_p is the specific heat of snow, ρ_p is the snow density, T_p is the snow temperature, λ_p is the thermal conductivity of the snow (0·3 W m^{-1} K^{-1}), I_n is the flux density of the net solar radiation entering the snow, ℓ_f is the heat of fusion of ice ($3{\cdot}34 \times 10^5$ J kg^{-1}), F is the snowmelt within the snow layer, t is time, and z is depth. The flux density of solar radiation is written as

$$\frac{\partial I_n}{\partial z} = -\mu(1 - \mathrm{ref}_s) S_d^{\downarrow} \exp(-\mu z) \tag{23}$$

where ref$_s$ is the albedo of snow and μ is the attenuation coefficient of solar radiation, which is kept constant (40 m^{-1}) (Fukami *et al.*, 1985). The simple method of Bai and Ohata (1989) is used to determine the snow albedo as

$$\mathrm{ref}_s = 1{\cdot}0118 \exp(-1{\cdot}954 \rho_p) \tag{24}$$

The snow density ρ_p is calculated using a simplified equation of Yamazaki *et al.* (1991):

$$\frac{\partial \rho_p}{\partial t} = \frac{W}{\eta'} \rho_p \tag{25}$$

where W is the weight of snow. η' can be written as

$$\eta' = A\eta_0 \exp(K\rho_p - \alpha_s T_s) \tag{26}$$

where η_0 is a constant ($6{\cdot}9 \times 10^5$ kg s m^{-2}), K is a constant ($2{\cdot}1 \times 10^{-2}$ m^3 kg^{-1}), and α_s is a constant ($9{\cdot}58 \times 10^{-2}$ °C^{-1}).

$$A = \frac{\exp(-\beta_s\omega_s) - \exp(-100\beta_s)}{1 - \exp(-100\beta_s)} \tag{27}$$

where ω_s is the water content of snow and β_s (18) is a constant.

The basic equation for thermal conduction in the soil layer is as follows (Outcalt *et al.*, 1975):

$$\frac{\partial T_g}{\partial t} = \frac{\partial}{\partial z}\left(\frac{\kappa}{c_g\rho_g}\frac{\partial T_g}{\partial z}\right) \tag{28}$$

where T_g is the soil temperature, κ is the thermal conductivity of soil, c_g is the specific heat of soil, and ρ_g is the soil density. Fukuda and Ishizaki (1980) consider that the phase change of soil water with thawing and freezing, specifically $A = \kappa/(c_g\rho_g)$ with a small finite temperature range ΔT can be replaced by

$$A = \frac{\kappa_1}{c_{g1}\rho_g} \qquad \text{if } T_g \le -\frac{\Delta T}{2} \quad \text{(frozen)} \tag{29}$$

$$A = \frac{\kappa_2}{\ell_f M + \frac{1}{2}(c_{g2}\rho_g + c_{g1}\rho_g)} \qquad \text{if } -\frac{\Delta T}{2} < T_g < \frac{\Delta T}{2} \quad \text{(phase transition)} \tag{30}$$

$$A = \frac{\kappa_2}{c_{g2}\rho_g} \qquad \text{if } T_g \ge \frac{\Delta T}{2} \quad \text{(unfrozen)} \tag{31}$$

where κ_1 is the thermal conductivity of frozen soil ($1{\cdot}2$ W m^{-1} K^{-1}), κ_2 is the thermal conductivity of unfrozen soil ($1{\cdot}0$ W m^{-1} K^{-1}), $c_{g1}\rho_g$ is the heat capacity of frozen soil, $c_{g2}\rho_g$ is the heat capacity of unfrozen soil, and M is the soil moisture content. Fukuda and Ishizaki (1980) also assumed that the temperature of the isothermal layer forming the lower boundary of the thermal conductive model, which is set at a depth of 6 m below the ground surface, equals the annual air temperature 2 m above the land surface. The soil layer and snowpack are subdivided at 0·01 m intervals in the study. An iterative process was used in the calculation and the value of convergence was set to 0·001 °C for the surface temperature difference between the current and previous result.

The runoff formation for a grid was simulated using a runoff model (Ma *et al.*, 2000) that is a modification of HYCYMODEL, developed by Fukushima (1988). The model input was effective precipitation P_n, which is the total amount of precipitation and snowmelt minus the evapotranspiration calculated using the SVAT model. The total runoff for a grid was calculated using four reservoirs to give surface runoff and base runoff. The modified HYCYMODEL used to produce each runoff component from the output of the SVAT model is shown in Figure 4 and is briefly summarized as follows:

$$S_c = K_c Q_c^{0{\cdot}6} \tag{32}$$

$$S_h = K_h Q_h^{0{\cdot}6} \tag{33}$$

$$S_u = K_u Q_u \tag{34}$$

$$S_b = K_b Q_b^{0{\cdot}1} \tag{35}$$

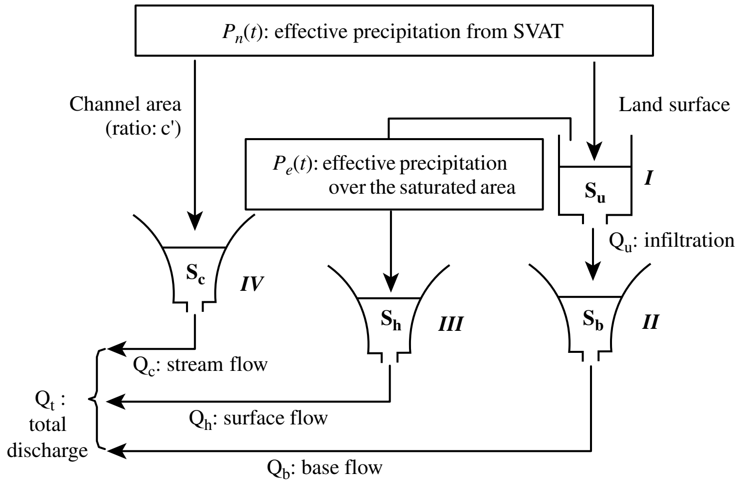

Figure 4. Sketch of the modified HYCYMODEL (from Ma *et al.* (2000). (Reproduced by permission of John Wiley & Sons Ltd.))

where S_c, S_h, S_u, and S_b are the storage in the channel, land surface, top soil layer and deep soil layer respectively, Q_c is the runoff from the channel area, Q_h is the runoff from the saturated area, Q_u is the infiltration from the top soil layer to the deep soil layer, and Q_b is the base flow from the deep soil layer. K_c, K_h, K_u, and K_b are constants. The storage change for each reservoir can be calculated as follows:

$$S_c(t) = S_c(t-1) + P_n(t) - Q_c(t) \qquad \text{when } P_n(t) \geq 0 \tag{36}$$

$$S_h(t) = S_h(t-1) + P_e(t) - Q_h(t) \qquad \text{when } P_n(t) \geq 0 \tag{37}$$

$$S_u(t) = S_u(t-1) + P_n(t) - P_e(t) - Q_u(t) \tag{38}$$

$$S_b(t) = S_b(t-1) + Q_u(t) - Q_b(t) \tag{39}$$

where t is the current time step and $t-1$ is the previous time step. $P_e(t)$ is the effective precipitation over the saturated area and is determined by the mean effective soil depth, D_{50} (mm), and its deviation D_{sig}. D_{sig} is defined as a constant (dimensionless number equal to 5), whereas D_{50} varies according to soil type. From previous studies (Nakashima and Fukushima, 1994; Tanaka *et al*., 1998), the value of D_{50} ranges from 25 mm for bare land to 120 mm for forested areas. In order to consider permafrost, D_{50} was defined using the following relationship with the depth of the active layer:

$$D_{50} = \alpha D_{a1} \tag{40}$$

where α (500) is a constant representing soil porosity and D_{a1} is the depth of the active layer. The value of $P_e(t)$ was calculated using

$$P_e(t) = mP_n(t) \tag{41}$$

where m is the saturated area ratio estimated as

$$m = \int_{-\infty}^{\chi} \frac{1}{\sqrt{2\pi}} \exp\left(\frac{\chi^2}{2}\right) d\chi \tag{42}$$

where χ is a parameter for the normal distribution defined as

$$\chi = \frac{\log[S'_u(t)/D_{50}]}{D_{sig}} \tag{43}$$

and

$$S_u'(t) = S_u(t-1) + P_n(t) \tag{44}$$

Note that if $P_n(t)$ is less than zero, then the value of $P_n(t)$ is first added to the topsoil storage as the evapotranspiration loss (Equation (34)). When the remaining topsoil storage is insufficient to offset the value of $P_n(t)$, the topsoil storage is set to zero and the remaining amount of $P_n(t)$ is deducted from the groundwater storage (Equation (35)). The total discharge Q_t, from a grid is then given by

$$Q_t = (1 - c')(Q_h + Q_b) + c'Q_c \tag{45}$$

where c' is the ratio of the impermeable area of the channel surface to the area of the watershed (equal to 0·05). The discharge enters the river network and then flows downstream.

The St Venant equations within a one-dimensional framework give a rigorous description of the open-channel flow in a river network (Beven and Wood, 1993). The St Venant equations can be solved using a finite-difference method. However, this necessitates specifying both the upstream and downstream boundary conditions, as well as the lateral inflow (e.g. Ma and Cheng, 1996). So far, this cannot be done on a macro-basin scale. The Muskingum method, a linear flood routing method, is used to estimate the river flow from upstream to downstream. To obtain the parameters used in the Muskingum model for each fixed river course requires data from many flood events. To simplify flow estimates for a river network, the velocity of river flow is set as a constant. This method has been used in Wyss *et al.* (1990), Naden (1993), Liston *et al.* (1994), Kite *et al.* (1994), Miller *et al.* (1994), Kanae *et al.* (1995), and Oki *et al.* (1996, 1999). Wyss *et al.* (1990) and Naden (1993) used a channel velocity of 0·6 m s^{-1} for small basins (area less than 10 000 km^2). Kite *et al.* (1994) predicted a velocity of 0·33 m s^{-1} for an impervious area (10 × 10 km^2 grid) in the Mackenzie River basin. Since the velocity varies with the grid scale, the value of the velocity in previous studies ranges from 0·2 to 0·6 m s^{-1}. Here, we assumed a constant velocity of 0·4 m s^{-1} for the Selenge River basin, which equalled the velocity used in the Lena River (Ma *et al.*, 2000). Moreover, it must be pointed out that the output of the SVAT and runoff models was for a 1° × 1° grid, and this was redistributed into a channel network using a 0·1° × 0·1° subgrid.

This model was applied to the Lena River basin in GAME (GEWEX Asian Monsoon Experiment)-Siberia (Ma *et al.*, 2000) and to the Torne–Kalix basin in the Project for the Intercomparison of Land-surface Parameterization Schemes Phase 2e (PILPS 2e) (Bowling *et al.*, 2003; Nijssen *et al.*, 2003). Ma and Fukushima (2002) described the model in detail and provided the model program codes. Figure 5 shows the model framework.

MODEL APPLICATION AND RESULTS

The model was applied to the Selenge River basin. To calibrate the model, the data for the first 2 years (1988 and 1989) were used. From the meteorological data, the amount of precipitation at all gauges was close to the annual level and no extreme climatic events occurred during the 2 years. The initial value of r_{smin} was set at 400 s m^{-1} for each grid and then the model was run for the 2 years. Then, the value of RDI for each grid was derived from the heat flux calculated in the initial run. According to Ma *et al.* (1999), the value of r_{smin} can be fixed by adjusting the slope of the linear relationship between r_{smin} and RDI until a reasonable hydrograph is obtained at the four hydrological gauges. In this study, the value of the slope η was fixed at 210. Consequently, the value of RDI for the basin ranged from 1·10 to 2·71, so r_{smin} ranged from 231 to 570 s m^{-1}. Table III shows the main parameters calibrated in this study and the corresponding values for other regions.

The model was then run for the verification period, 1990 to 1992. Figure 6 compares the observed and calculated results of the daily hydrographs at the four hydrological gauges in the basin. The calculated hydrographs are close to those observed throughout the calibration period (1988–89), except for missing

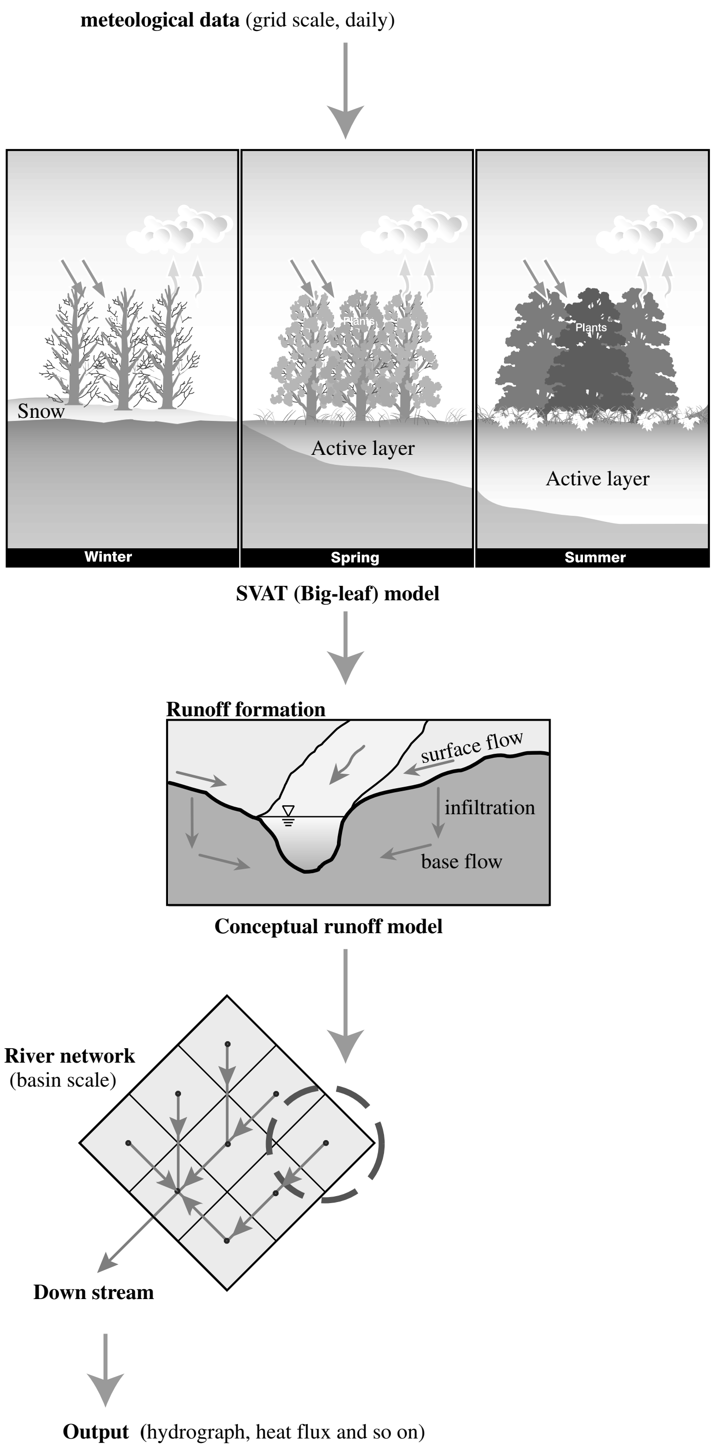

Figure 5. Flowchart of the model

Table III. Calibrated parameters used in the model and those variation in different regions

Parameter	Unit	Lena River basin (Ma *et al.*, 2000)	PILPS 2e (Bowling *et al.*, 2003; Nijssen *et al.*, 2003)	Selenge River basin (this study)
η	—	135	200	210
K_b	$mm^{9/10}h^{1/10}$	687	687	687
K_u	h	21·7	10	40·7
K_h	$mm^{2/5}h^{3/5}$	10	20	5
K_e	$mm^{2/5}h^{3/5}$	2	2	2

data for no. 14 in 1989. From 1990 to 1992, the hydrograph at gauge no. 1 was relatively stable. However, the hydrographs at gauges no. 3 and no. 14 fluctuated over the 3 years, especially in 1990, which was wetter than the other years. Except for gauge no. 4, which was missing data, the flow due to snowmelt far exceeded the values observed in 1990 at all gauges. The simulated hydrographs for 1991 had a time lag at all gauges compared with the observed hydrographs, whereas for 1990 they overestimated the observed values at gauges no. 1 and no. 3, and underestimated them at no. 14 during the summer. In contrast, the simulated hydrographs for 1992 at gauge nos 1, 3, and 4 were underestimates of the observed values. For the water budget, the annual precipitation throughout the basin was 298 mm and the estimated evapotranspiration was 241 mm; the difference was 57 mm. The calculated annual runoff at gauge no. 4 was 50 mm (the data were missing for 1990–91).

ANALYSIS AND DISCUSSION

The annual average sunshine in Mongolia is around 3000 h, which is longer than in other countries at the same latitude. The predicted capacity for evapotranspiration is, therefore, much higher than in other regions. Using our model, a preliminary water budget was obtained. Table IV shows the distribution of the 5 year average annual precipitation calculated with the data from the 10 gauges and extrapolated to the $1^\circ \times 1^\circ$ grid for the entire basin using distance-related interpolation. The annual precipitation was 298 mm and ranged from 212 to 352 mm. Oyunbaatar (1999, 2001) reported that the geographic conditions in the Selenge River basin vary markedly, as does the amount and spatial distribution of precipitation. The difference in precipitation, 140 mm, is not very large, and may have been smoothed as a result of using interpolation to calculate $1^\circ \times 1^\circ$ grids from the precipitation at 10 gauges. Table IV also lists the estimated annual evapotranspiration during the period. The evapotranspiration averaged 241 mm, and ranged from 153 to 300 mm. In addition, Table IV shows the estimated potential evapotranspiration (with $r_{smin} = 0$). The minimum was 1096 mm and the maximum was 2779 mm. The basin average was 2009 mm. Table V shows the distribution of the ratio of annual evapotranspiration to precipitation. The basin average was 0·81, with a range between 0·64 and 0·96. Therefore, about 81% of the precipitation is lost to evapotranspiration. In other words, the runoff ratio (annual runoff to precipitation) of the basin is 0·19, which is far lower than the reported values of 0·49–0·80 for Japan (Ma *et al.*, 1999), 0·26–0·58 for major Eurasian rivers (Serreze *et al.*, 2001), and 0·58 for the Mackenzie River (Kite *et al.*, 1994).

These results show that evapotranspiration dominates the hydrological cycle in the basin. The method used to estimate the amount of evapotranspiration is, therefore, key to increasing the accuracy of the hydrological simulation. Table V also shows the dimensionless ratio of actual evapotranspiration to potential evapotranspiration; it averaged 0·12, with a range from 0·07 to 0·18. Moreover, Table V shows the value of the wetness index (annual precipitation to potential evapotranspiration) for the basin, which averaged 0·15 and ranged between 0·1 and 0·24. This is an important index for classifying climate regions (Kondo and Xu,

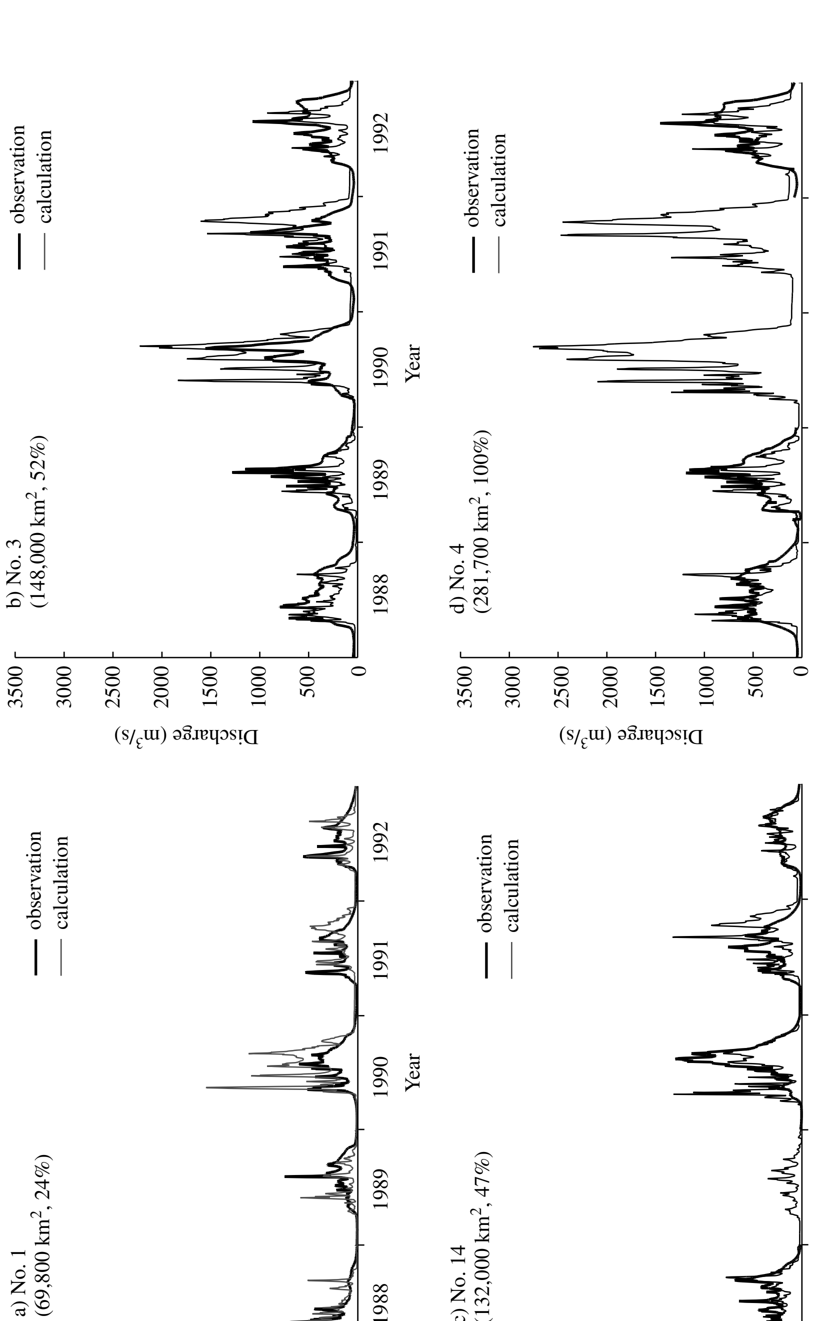

Figure 6. Comparison of observed and calculated hydrographs at four hydrological stations from 1988 to 1992. The catchment area and its percentage of the whole basin are indicated in parentheses

Table IV. Spatial distribution of annual precipitation (mm), evapotranspiration (mm), and potential evapotranspiration (mm) over the basin in 1° × 1° grids based on data for 10 gauges during the period 1988–92

N\E	96°	97°	98°	99°	100°	101°	102°	103°	104°	105°	106°	107°	108°
Estimated annual precipitation													
51°					299	324							
50°			292	304	306	300	332	339	343	332	324		
49°		270	268	253	251	303	330	347	352	336	319	310	
48°	265	265	262	264	273	312	329	326	350	317	300	298	300
47°	264	263	265	279	320	341	301	286	309	290	290	290	
46°					212	272	273	275	276	275			
Estimated evapotranspiration													
51°					201	213							
50°			202	194	221	232	247	249	276	295	289		
49°		182	205	217	227	245	268	280	295	300	277	279	
48°	199	214	204	225	221	248	257	271	296	273	255	238	232
47°	202	187	180	211	224	270	283	276	288	259	250	240	
46°					153	210	252	257	256	263			
Estimated potential evapotranspiration													
51°					1857	1591							
50°			1842	1751	2037	2240	1751	1587	1893	2424	2630		
49°		1713	2061	2503	2779	1997	1627	1745	1931	2388	2526	2529	
48°	1324	1682	1837	2158	2288	1905	1611	1727	1936	2428	2551	2210	2014
47°	1117	1096	1368	1732	1861	2180	2254	2349	2073	2675	2690	2335	
46°					2138	1631	1638	1884	2033	2334			

1997). According to Kondo and Xu (1997), the value of the index is between 0·1 and 0·3 for semi-arid areas; therefore, according to this criterion, the basin is a semi-arid region.

This study estimated evapotranspiration using the Penman–Monteith method (Monteith, 1965) using the heat balance and assumptions for local conditions. The minimum surface resistance r_{smin} was calibrated especially carefully, although a simple method (Blyth and Harding, 1995) of estimating the surface resistance r_{s} was used for the basin. Nijssen *et al*. (1997) and Abdulla and Lettenmaier (1997) indicated that hydrological simulations of arid and semi-arid basins are difficult, even when using the SVAT-coupled model, VIC-2L (Liang *et al*., 1994). Nijssen *et al*. (1997) referenced the dataset of minimum surface resistance of Sellers *et al*. (1994) for their study area. The dataset of Sellers *et al*. (1994) is very important global-scale vegetation information used for general circulation models, but more detail is necessary for a specific region (e.g. Unland *et al*., 1996). Based on a hydrological analysis, Ma *et al*. (1999) reported an average value of 60 s m^{-1} for a forested mountainous catchment in central Japan and Ma *et al*. (2000) reported values of 78 to 911 s m^{-1} in the Lena River basin for a 1° × 1° grid. For the Torne–Kalix basin (an experimental basin for PILPS 2(e) located in northern Scandinavia), values of r_{smin} were derived that ranged from 57 to 126 s m^{-1} at a spatial resolution of 0·25°.

The accuracy of the extended meteorological data is not discussed, because it is very difficult to obtain results for the basin using data from only 10 gauges. The density of gauges in Mongolia is low; it equals 1/5080 km^2, which is 2·5 times less than the WMO standard for rainfall observations (Oyunbaatar, 1999). Michaud and Sorooshian (1994b) recommended that the density of rain gauges should be not less than 4 km^2 per gauge for semi-arid catchments, because the amount of precipitation directly affects the hydrological response. In addition, some digital data for the basin should be checked more carefully. Table VI shows the February precipitation measured at nine rain gauges in the basin over the 5 years (gauge no. 236 has missing data during this period). The values for 1990 are three times larger than those for other years, except at gauges

Table V. Spatial distribution of ratio of evapotranspiration (annual evapotranspiration to precipitation), dimensionless evapotranspiration (estimated actual evapotranspiration to potential evapotranspiration), and wetness index (annual precipitation to potential evapotranspiration) for the basin in the period 1988–92

N\E	96°	97°	98°	99°	100°	101°	102°	103°	104°	105°	106°	107°	108°
Evapotranspiration ratio													
51°					0·67	0·66							
50°			0·69	0·64	0·72	0·77	0·74	0·74	0·81	0·89	0·89		
49°		0·67	0·77	0·86	0·91	0·81	0·81	0·81	0·84	0·89	0·87	0·90	
48°	0·75	0·81	0·78	0·85	0·81	0·79	0·78	0·83	0·85	0·86	0·85	0·80	0·77
47°	0·77	0·71	0·68	0·76	0·70	0·79	0·94	0·96	0·93	0·89	0·86	0·83	
46°					0·72	0·77	0·93	0·94	0·93	0·96			
Dimensionless evapotranspiration													
51°					0·11	0·13							
50°			0·11	0·11	0·11	0·10	0·14	0·16	0·15	0·12	0·11		
49°		0·11	0·10	0·09	0·08	0·12	0·17	0·16	0·15	0·13	0·11	0·11	
48°	0·15	0·13	0·11	0·10	0·10	0·13	0·16	0·16	0·15	0·11	0·10	0·11	0·12
47°	0·18	0·17	0·13	0·12	0·12	0·12	0·13	0·12	0·14	0·10	0·09	0·10	
46°					0·07	0·13	0·15	0·14	0·13	0·11			
Wetness index													
51°					0·16	0·20							
50°			0·16	0·17	0·15	0·13	0·19	0·21	0·18	0·14	0·12		
49°		0·16	0·13	0·10	0·09	0·15	0·20	0·20	0·18	0·14	0·13	0·12	
48°	0·20	0·16	0·14	0·12	0·12	0·16	0·20	0·19	0·18	0·13	0·12	0·14	0·15
47°	0·24	0·24	0·19	0·16	0·17	0·16	0·13	0·12	0·15	0·11	0·11	0·12	
46°					0·10	0·17	0·17	0·15	0·14	0·12			

Table VI. Comparison of precipitation at various gauges in February for two different period: period A, the 4 year average for 1988 to 1992, excluding 1990; period B, amount for 1990

	Precipitation (mm)								
Period	207	231	232	272	282	285	287	290	292
A	3·2	2·4	2·5	3·2	3·5	4·1	5·1	2·2	2·9
B	18·0	2·0	2·0	77·0	30·0	45·0	22·0	95·0	33·0

no. 231 and 232, yet the observed hydrographs indicate that those heavy precipitation events (snowfall) did not lead to a big spring flood compared with other years.

CONCLUSION

A hydrological study was carried out for the Selenge River basin, the biggest source of freshwater in Mongolia, using a scheme for the interaction between the land surface and atmosphere coupled with a hydrological model, using data for 1988 to 1992. The results demonstrated that it was possible to model the hydrological processes, based on comparisons of the observed and calculated hydrographs at four hydrological stations. Using the results, the basin-scale distribution of the water budget components was examined. The extended annual precipitation was 298 mm and ranged from 212 to 352 mm, whereas the estimated evapotranspiration averaged 241 mm and ranged from 153 to 300 mm. This is a high-evapotranspiration area; about 81% of precipitation is lost via evapotranspiration. This study determined that the annual potential evapotranspiration over the basin averaged 2009 mm, and ranged from 1096 to 2779 mm. The dimensionless ratio of evapotranspiration (annual evapotranspiration to potential evapotranspiration) averaged 0·12 and ranged between 0·07 and 0·18. The wetness index (annual precipitation to potential evapotranspiration) averaged 0·15 and ranged between 0·1 and 0·24, clearly indicating that the basin should be classified as a semi-arid region. By contrast, the value of r_{smin} ranged between 231 and 570 s m^{-1} for the basin at a 1° resolution; this information should prove useful for studies of hydrology and climatology related to climate change in the region.

ACKNOWLEDGMENTS

This work is part of a cooperative research program examining water and energy cycles in Mongolia by the Frontier Observational Research System, Japan, and the Institute of Meteorology and Hydrology, Mongolia. We thank Professor Yoshihiro Fukushima, Research Institute for Humanity and Nature, Japan, for his valuable comments on this paper.

REFERENCES

Abdulla FA, Lettenmaier DP. 1997. Application of regional parameter estimation schemes to simulate the water balance of a large continental river. *Journal of Hydrology* **197**(1–4): 258–285.

Adyabadam G. 1999. Socio-economic value of water resources. In *Papers in Meteorology and Hydrology* No. 21/2, Davaa G, Natsagdorj L, Dagvadorj D (eds). Institute of Meteorology and Hydrology: Ulaanbaatar, Mongolia; 116–121.

Andersen J, Refsgaard JC, Jensen KH. 2001. Distributed hydrological modeling of the Senegal River Basin—model construction and validation. *Journal of Hydrology* **247**: 200–214.

Bai Z, Ohata T. 1989. Variation of albedo on the Glacier No. 1 at the headwater of Urumqi River, Tianshan Mountains, during the summer ablation period. *Journal of Glaciology and Geocryology* **11**: 311–324 (in Chinese).

Beven K, Wood EF. 1993. Flow routing and the hydrological response of channel networks. In *Channel Network Hydrology*, Beven K, Kirkby MJ (eds). John Wiley & Sons: Chichester; 99–128.

Blyth EM, Harding RJ. 1995. Application of aggregation models to surface heat flux from the Sahelian tiger bush. *Agricultural and Forest Meteorology* **72**: 213–235.

Bowling LC, Lettenmaier DP, Nijssen B, Graham PL, Clark D, Maayar ME, Essery R, Goers S, Gusev Y, Habets F, Hurk B, Jing J, Kahan D, Lohmann D, Ma X, Mahanama S, Mocko D, Nasonova O, Samuelsson P, Shmakin AB, Takata K, Verseghy D, Viterbo P, Xue Y, Yang Z. 2003. Simulation of high latitude hydrological processes in the Torne–Kalix basin: PILPS Phase 2(e) 1: Experiment description and summary intercomparisons. *Global and Planetary Change* **38**: 1–30.

Dagvadorj D. 2000. Introduction. In *Mongolia National Action Programme on Climate Change*, Batjargal Z, Dagvadorj D, Batima P (eds). JEMR Publishing: Mongolia; 1–11.

Dagvadorj D, Batjargal Z. 1999. Response actions to address climate change problems in Mongolia. In *Papers in Meteorology and Hydrology* No. 21/2, Davaa G, Natsagdorj L, Dagvadorj D (eds). Institute of Meteorology and Hydrology: Ulaanbaatar, Mongolia; 3–16.

Fukami H, Kojima K, Aburak-awa H. 1985. The extinction and absorption of solar radiation within a snow cover. *Annals of Glaciology* **6**: 118–122.

Fukuda M, Ishizaki T. 1980. A simulation model for frost penetration beneath the ground on the basis of equilibrium surface temperatures. *Journal of Japan Society of Snow and Ice* **42**: 71–80 (in Japanese with English abstract).

Fukushima Y. 1988. A model of river flow forecasting for a small forested mountain catchment. *Hydrological Processes* **2**: 167–185.

Jarvis PG. 1976. The interpretation of the variations in leaf water potential and stomatal conductance found in canopies in the field. *Philosophical Transactions of the Royal Society of London, Series B: Biological Sciences* **273**: 593–610.

Jothityangkoon C, Sivapalan M, Farmer DL. 2001. Process controls of water balance variability in a large semi-arid catchment: downward approach to hydrological model development. *Journal of Hydrology* **254**: 174–198.

Kanae S, Nishio K, Oki T, Musiake K. 1995. Hydrograph estimations by flow routing modelling from AGCM output in major basins of the world. *Annual Journal of Hydraulic Engineering, JSCE* **39**: 97–102 (in Japanese with English abstract).

Kite GW, Dalton A, Dion K. 1994. Simulation of streamflow in a macroscale watershed using general circulation model data. *Water Resources Research* **30**(5): 1547–1559.

Kondo J. 1994. *Meteorology of Water Environment*. Asakura: Tokyo (in Japanese).

Kondo J, Xu J. 1997. Heat and water balances of the ground surface in China (4): potential evaporation and wetness index. *Journal of the Japan Society of Hydrology and Water Resources* **10**: 458–462 (in Japanese with English abstract).

Lange L, Leibundgut C, Greenbaum N, Schick P. 1999. A noncalibrated rainfall-runoff model for large, arid catchments. *Water Resources Research* **35**(7): 2161–2172.

Liang X, Lettenmaier DP, Wood EF, Burges SJ. 1994. A simple hydrologically based model of land surface water and energy fluxes for general circulation models. *Journal of Geophysical Research* **99**(D7): 14 415–14 428.

Liston GE, Sud YC, Wood EF. 1994. Evaluating GCM land surface hydrology parameterizations by computing river discharges using a runoff routing model: application to the Mississippi basin. *Journal of Applied Meteorology* **33**: 394–405.

Ma X, Cheng W. 1996. A modeling of hydrological processes in a large low plain area including lakes and ponds. *Journal of the Japan Society of Hydrology and Water Resources* **9**: 320–329.
Ma X, Fukushima Y. 2002. Numerical model of river flow formation from small to large scale river basins. In *Mathematical Models of Large Watershed Hydrology*, Singh VP, Frevert DK (eds). Water Resources Publications: Highlands Ranch, CO; 433–470.
Ma X, Hiyama T, Fukushima Y, Hashimoto T. 1998. A numerical model of the heat transfer for permafrost regions. *Journal of the Japan Society of Hydrology and Water Resources* **11**: 346–359.
Ma X, Fukushima Y, Hashimoto T, Hiyama T, Nakashima T. 1999. Application of a simple SVAT model in a mountain catchment under temperate humid climate. *Journal of the Japan Society of Hydrology and Water Resources* **12**: 285–294.
Ma X, Fukushima Y, Hiyama T, Hashimoto T, Ohata T. 2000. A macro-scale hydrological analysis of the Lena River basin. *Hydrological Processes* **14**: 639–651.
Manabe S, Stouffer RJ, Spelman MJ, Bryan K. 1991. Transient response of a coupled ocean–atmosphere model to a gradual change of atmospheric CO_2, part I: annual mean response. *Journal of Climate* **4**: 785–818.
McMahon TA. 1988. Drought and arid zone hydrology. *Civil Engineering Transactions* **30**(4): 175–185.
Michaud J, Sorooshian S. 1994a. Comparison of simple versus complex distributed runoff models on a midsized semiarid watershed. *Water Resources Research* **30**(3): 593–605.
Michaud J, Sorooshian S. 1994b. Effect of rainfall-sampling errors on simulations of desert flash floods. *Water Resources Research* **30**(10): 2765–2775.
Miller JR, Russell GL, Caliri G. 1994. Continental-scale river flow in climate models. *Journal of Climate* **7**: 914–928.
Milly PCD. 1992. Potential evaporation and soil moisture in general circulation models. *Journal of Climate* **5**: 209–225.
Milly PCD. 1997. Sensitivity of greenhouse summer dryness to changes in plant rooting characteristics. *Geophysical Research Letters* **24**: 269–271.
Monteith JL. 1965. Evaporation and environment. In *The Stage and Movement of Water in Living Organisms*, Fogg GE (ed.). Symposia of the Society for Experimental Biology, vol. 19. Cambridge University Press: Cambridge; 205–234.
Naden PS. 1993. A routing model for continental-scale hydrology. In *Macroscale Modelling of the Hydrosphere*, Wilkinson WB (ed.). IAHS Publication no. 214. IAHS Press: Wallingford; 67–79.
Nakashima T, Fukushima Y. 1994. Characteristics of streamflow at two source watersheds of the Yura river in highland area of Kyoto University Forest in Ashiu. *Bulletin of the Kyoto University Forests* **66**: 61–75 (in Japanese with English summary).
Nijssen B, Lettenmaier DP, Liang X, Wetzel SW, Wood EF. 1997. Streamflow simulation for continental-scale river basins. *Water Resources Research* **33**(4): 711–724.
Nijssen B, Bowling LC, Lettenmaier DP, Clark DB, Maayar ME, Essery R, Goers S, Gusev Y, Habets F, Hurk B, Jing J, Kahan D, Lohmann D, Ma X, Mahanama S, Mocko D, Nasonova O, Niu G, Samuelsson P, Shmakin AB, Takata K, Verseghy D, Viterbo P, Xia Y, Xue Y, Yang Z. 2003. Simulation of high latitude hydrological processes in the Torne–Kalix basin: PILPS Phase 2(e) 2: Comparison of model results with observations. *Global and Planetary Change* **38**: 31–53.
Oki T, Kanae S, Musiake K. 1996. River routing in the global water cycle. *GEWEX News* **6**(3): 4–5.
Oki T, Nishimura T, Dirmeyer P. 1999. Assessment of annual runoff from land surface models using Total Runoff Integrating Pathways (TRIP). *Journal of the Meteorological Society of Japan* **77**: 235–255.
Outcalt SI, Goodwin C, Weller G, Brown J. 1975. Computer simulation of the snowmelt and soil thermal regime at Barrow, Alaska. *Water Resources Research* **11**: 709–715.
Oyunbaatar D. 1999. Spatial rainfall analysis in the Selenge River basin. In *Papers in Meteorology and Hydrology* No. 21/2, Davaa G, Natsagdorj L, Nagvadorj D (eds). Institute of Meteorology and Hydrology: Ulaanbaatar, Mongolia; 122–139.
Oyunbaatar D. 2001. Runoff and rainfall distribution in the Selbe river basin. In *Proceedings of the International Workshop on GAME–ANN/Radiation*, Thailand; 102–106.
Renard KG, Lane LJ, Simanton JR, Emmerich WE, Stone JJ, Weltz MA, Goodrich DC, Yakowitz DS. 1993. Agricultural impacts in an arid environment: Walnut Gulch studies. *Hydrological Science and Technology* **9**(1–4): 145–190.
Sellers PJ, Los SO, Tucker CJ, Justice CO, Dazlich DA, Collatz GJ, Ranfall DA. 1994. A global 1 by 1 degree NDVI data set for climate studies, 2, the generation of global fields of terrestrial biophysical parameters from the NDVI. *International Journal of Remote Sensing* **15**(17): 3519–3545.
Serreze MC, Clark MP, Etringer AJ, Bromwich DH. 2001. Variability and trends in the hydro-climatology of the major Eurasian arctic drainages. In *Proceedings of Second Wadati Conference on Global Change and Polar Climate*, Tsukuba, Japan; 83–86.
Tanaka H, Fukushima Y, Li C, Kubota J, Ohta T, Suzuki M, Kosugi K. 1998. Water discharge property of evergreen broad-leaved forest river basin—Jiulianshan, Jiangxi Province, China. *Journal of the Japan Society of Hydrology and Water Resources* **11**: 240–252.
Unland HE, Houser PR, Shuttleworth WJ, Yang Z. 1996. Surface flux measurement and modeling at a semi-arid Sonoran Desert. *Agricultural and Forest Meteorology* **82**: 119–153.
Verstraete M, Schwartz SA. 1991. Desertification and global change. In *Vegetation and Climate Interactions in Semi-arid Regions*, Henderson-Sellers A, Pitman AJ (eds). Kluwer Academic Publishers: Dordrecht, The Netherlands; 3–13.
Wetherald RT, Manabe S. 1999. Detestability of summer dryness caused by greenhouse warming. *Climatic Change* **43**: 495–511.
Wetherald RT, Manabe S. 2002. Simulation of hydrologic changes associated with global warming. *Journal of Geophysical Research* **107**(D19): 4379, doi:10.1029/2001JD001195.
Wyss J, Williams ER, Bras RL. 1990. Hydrologic modelling of New England river basins using radar rainfall data. *Journal of Geophysical Research* **95**: 2143–2150.
Yamazaki T, Sakuraoka T, Nakamura T, Kondo J. 1991. A study of snow metamorphism: I. Model description. *Journal of the Japan Society of Snow and Ice* **53**: 115–123 (in Japanese with English abstract).
Ye W, Bates BC, Viney NR, Sivapalan M, Jakeman AJ. 1997. Performance of conceptual rainfall-runoff models in low-yielding ephemeral catchments. *Water Resources Research* **33**(1): 153–166.

